Pathogenesis of wild-type- and vaccine-based recombinant peste des petits ruminants virus (PPRV) expressing EGFP in experimentally infected domestic goats

Katharina S. Schmitz[1]†, Phaedra L. Eblé[2]†, René G. P. van Gennip[2], Mieke A. Maris-Veldhuis[2], Rory D. de Vries[1], Lucien J. M. van Keulen[3], Rik L. de Swart[1,2,*,†] and Piet A. van Rijn[2,4,*,†]

Abstract

Peste des petits ruminants virus (PPRV) is a highly contagious morbillivirus related to measles and canine distemper virus, mostly affecting small ruminants. The corresponding PPR disease has a high clinical impact in goats and is characterized by fever, oral and nasal erosions, diarrhoea and pneumonia. In addition, massive infection of lymphoid tissues causes lymphopaenia and immune suppression. This results in increased susceptibility to secondary bacterial infections, explaining the observed high mortality in some outbreaks. We studied the pathogenesis of PPR by experimental inoculation of Dutch domestic goats with a recombinant virulent PPRV strain modified to express EGFP and compared it to an EGFP-expressing vaccine strain of PPRV. After intratracheal inoculation with virulent PPRV, animals developed fever, viraemia and leucopaenia, and shed virus from the respiratory and gastro-intestinal tracts. Macroscopic evaluation of fluorescence at the peak of infection 7 days post-inoculation (dpi) showed prominent PPRV infection of the respiratory tract, lymphoid tissues, gastro-intestinal tract, mucosae and skin. Flow cytometry of PBMCs collected over time demonstrated a cell-associated viraemia mediated by infected lymphocytes. At 14 dpi, pathognomonic zebra stripes were detected in the mucosa of the large intestine. In contrast, vaccine strain-inoculated goats remained largely macroscopically fluorescence negative and did not present clinical signs. A low-level viraemia was detected by flow cytometry, but at necropsy no histological lesions were observed. Animals from both groups seroconverted as early as 7 dpi and sera efficiently neutralized virulent PPRV *in vitro*. Combined, this work presents a study of the pathogenesis of wild type- and vaccine-based PPRV in its natural host. This study shows the strength of recombinant EGFP-expressing viruses in fluorescence-guided pathogenesis studies.

INTRODUCTION

Peste des petits ruminants virus (PPRV) causes severe and often fatal disease in small ruminants such as goats or sheep. PPRV spreads via the respiratory tract and is highly contagious [1]. Clinical manifestations include fever, ocular and nasal discharges, diarrhoea, or respiratory signs such as pneumonia or tracheitis [2]. PPRV is closely related to rinderpest virus (RPV) and belongs to the family *Paramyxoviridae*, genus *Morbillivirus*, which comprises multiple relevant human and veterinary pathogens including measles virus (MeV) and canine distemper virus (CDV) [3]. Similar to other morbilliviruses, PPRV causes depletion of lymphocytes from peripheral blood and lymphoid tissues, facilitating secondary bacterial infections and causing case fatality rates of up to 80–100% in severe outbreaks [4]. Since the eradication of RPV and the end of its vaccination programme in 2011, the percentage of ruminants with cross-protective immunity to PPRV is decreasing and PPRV surveillance is becoming of increasing interest and importance [5]. Phylogenetic analysis has identified four distinct PPRV lineages (I–IV), of which lineage IV is the

most prevalent [6]. PPRV causes extensive economic losses, especially in Africa and Asia [7, 8]. Next to enzootic circulation in Africa, the Middle East and Asia, PPRV is also a growing threat in Europe [9] as it has been detected in Georgia and Bulgaria in recent years [10, 11].

In 2015, PPRV was nominated by the World Organization for Animal Health (OIE) and Food and Agriculture Organization of the United Nations (FAO) for eradication by 2030 [12]. Multiple live-attenuated vaccines are available and are used in several countries with endemic PPRV circulation. The lineage II Nigeria 75/1 virus is the most widely used vaccine outside of India and was attenuated by more than 60 successive passages in Vero cells [13, 14]. Unfortunately, as a live-attenuated virus vaccine, it requires continuous cold-chain preservation, cannot be distinguished from a natural infection (no Differentiating between Infected and Vaccinated Animals [no DIVA-vaccine]) and may revert from attenuated to virulent on rare occasions.

Despite its recognized importance, little is known about the pathogenesis of virulent PPRV strains. In the last 20 years, a number of studies have evaluated PPRV isolates in diverse goat or sheep species, using various routes of inoculation and different timings [4, 15–26]. Those suggest that disease severity is linked to the PPRV strain [25, 26]. Moreover, PPR disease seems more severe in goats than in sheep, and more severe in young animals. As for other morbilliviruses [27], it was shown that immune cells in the respiratory tract are initial targets, which ensure viral dissemination throughout the body, affecting $CD4^+$, $CD8^+$ and $WC1^+$ T cells as well as $CD21^+$ B cells and MHC class II^+ cells which morphologically resemble cells of the monocyte lineage [19, 28]. Infection with PPRV induces a durable immune response; however, the presence of neutralizing antibodies often does not prevent death [29].

Knowledge of the mechanisms underlying PPR vaccine immunogenicity and efficacy is limited. Seroconversion can be seen as early as 7 days post-vaccination using a subcutaneous or nasal administration route [30], and PPR vaccine viruses are not shed [31]. Experimental vaccination leads to sterile immunity and induces humoral and cellular responses that protect against all four lineages [31]. The main correlate of protection seems to be antibodies and/or $CD4^+$ T cells, as sterile immunity is retained after $CD8^+$ T cell depletion post-vaccination [28]. However, the tropism of PPR vaccines is largely unknown.

The advantage of recombinant viruses expressing a reporter protein for *in vivo* pathogenesis studies of morbilliviruses has been extensively demonstrated [32–34]. Using this approach, virus-infected cells can be tracked on a macroscopic, microscopic and single-cell level. Here, we have studied the pathogenesis of virulent wild-type- and vaccine-based PPRV expressing EGFP in Dutch domestic goats. The virulent virus, based on PPRV/Georgia/Tbilisi/2016, infected the respiratory tract, lymphoid organs, alimentary tract and mucosa/skin, caused histological lesions and pathognomonic zebra stripes in the large intestine, but was self-limiting. The vaccine virus, based on the Nigeria 75/1 strain, induced a robust immune response despite causing only a short viraemic phase with limited virus detection at day 8.

METHODS

Viruses and cells

Vero cells expressing dog signalling lymphocyte activation molecule (SLAM) (VDS, a kind gift of Dr Y. Yanagi) [35], Vero cells expressing dog nectin-4 (VN4, a kind gift of Dr C. Richardson) and CV1 cells expressing goat SLAM (CHS-20) [36], kindly provided by Dr A. Bataille, were cultured in Dulbecco's modified Eagle's medium (DMEM; Fischer Scientific) containing 5% FBS, 100 IU ml^{-1} penicillin, 100 µg ml^{-1} streptomycin and 2.5 µg ml^{-1} amphotericin B (Fischer Scientific). Fowlpox virus expressing DNA dependent T7 RNA-polymerase (FPV-T7) was a kind gift of Dr M. Skinner [37], PPR vaccine strain PPRV/Nig75/1 (lineage II) was a kind gift of CIRAD, France, and virulent PPRV/Georgia/Tbilisi/2016 (lineage IV), isolated from lung tissue after two passages in VDS cells, was a kind gift of Dr C. Batten [38].

Virus stocks were generated by infection of CHS-20 cells at low m.o.i. and harvested when 100% cytopathic effect (CPE) was observed. Virus titres were determined by endpoint titration and expressed as TCID$_{50}$ ml^{-1}. Virus stocks were stored at −80 °C. For growth curves, recombinant PPR viruses expressing EGFP were compared with their parental strains. Confluent monolayers of CHS-20 cells in 24-well plates were infected at an m.o.i. of 0.1. After attachment to cells for 1.5 h at 37 °C, medium was removed and refreshed with 1 ml DMEM with 5% FBS and 2.5 µg ml^{-1} amphotericin B and incubation was continued. At indicated timepoints post-infection, the supernatant was harvested and stored at −80 °C. Harvests were freeze-thawed and titrated on CHS-20 cells in a ten-fold dilution series. Virus titres were expressed as TCID$_{50}$ ml^{-1}.

Construction of full-length cDNA of PPRV/Georgia/Tbilisi/2016

Four cDNA fragments covering the whole genome of PPRV/Georgia/Tbilisi/2016, GenBank accession number MF737202 [38], were synthesized by Genscript. cDNA fragments were of approximately the same length and contained cloning sites as present in PPRV/Georgia/Tbilisi/2016. The ORF of EGFP including a translation initiation sequence (Kozak sequence) was inserted between the P and M genes (position 3), flanked by sequences of the intergenic region between P and M, and was adjusted according to the rule-of-six for morbillivirus genomes [39]. The early promoter of human cytomegalovirus (P$_{HCMV}$) and the promoter of bacteriophage T7 (P$_{T7}$) were added followed by the hammerhead ribozyme sequence adjacent to the

5′-end of the PPRV-antigenome. Adjacent to the 3′-end, the hepatitis delta ribozyme followed by the polyA signal and the T7 transcription terminator were synthesized. In addition to internal unique cloning sites, cloning sites were situated outside the added features at the 5′- and 3′-end of the respective terminal cDNA fragments. A multiple cloning site with these sites was synthesized and cloned in plasmid pOK12 [40]. cDNA fragments were cloned, followed by subsequent extension with flanked fragments until full genome cDNA of PPRV with the EGFP cassette was achieved (Fig. S1, available with the online version of this article). To generate cDNA of PPRV without EGFP, the cassette was removed and replaced by the original sequence of PPRV/Georgia/Tbilisi/2016. As a result, P_{HCMV}- or P_{T7}-driven RNA transcripts resulted in antigenomic PPRV-RNA by cleavage of both ribozyme sequences.

Rescue of rPPRV

Expression plasmids of N, P and L proteins of PPRV/Nig75/1 and full-length cDNA of rPPRV/Nigeria-EGFP[3], based on PPRV/Nig75/1 expressing EGFP as an additional transcription unit at position 3 of the genome, were a kind gift of Dr A. Bataille. In total, 1 µg plasmids (0.5 µg plasmid with full-length cDNA, and 0.5 µg expression plasmids in equal amounts) in 50 µl Opti-MEM I Reduced Serum Medium were mixed with 2 µl P3000 Reagent (Invitrogen). This mix was added to a prepared mixture of 50 µl Opti-MEM I Reduced Serum Medium containing 2 µl Lipofectamine 3000 (Invitrogen) according to the manufacturer's suggestions. After incubation for 5 min at 20 °C, the transfection mix was dropwise added to monolayers of 10^5 VDS cells per 2 cm² (24-well) and incubated at 37 °C. Alternatively, VDS cell monolayers were first infected with FPV-T7 at an m.o.i. of 0.5. After 1.5 h, infected monolayers were transfected as described above. Rescue of rPPRV-EGFP was monitored using the digital inverted microscope EVOSfl (AMG) in the GFP channel. Rescued rPPRV was harvested from transfected monolayers developing CPE. Alternatively, transfected monolayers were passaged to increase the amount of rescued virus. Successful rescue was demonstrated by infection of fresh cell monolayers. Rescue of all rPPRV variants was also confirmed by immunostaining with monoclonal antibody C77 directed against the H protein (Pirbright Institute) in infected VDS cell monolayers fixed with methanol/aceton (1:1) according to standard procedures [41]. Virus stocks were prepared by two virus passages on CHS-20 cells.

Full genome sequencing of PPRV

PPRV-RNA of virus stocks was isolated using the High Pure Roche viral RNA kit according to the instructions of the supplier (Roche). Reverse transcription (RT) and PCR amplification was performed with appropriate sets of primers by the one-tube system (Qiagen one-step RT-PCR kit) or Superscript IV-one step RT-PCR kit (Invitrogen) to amplify overlapping cDNA fragments (Table S1). DNA fragments were purified using a High Pure PCR product purification kit (Roche) and were pooled to equimolar amounts at a concentration of 50 ng µl⁻¹ and submitted for next generation sequencing (NGS). NGS libraries were constructed using Illumina's Nextera DNA Flex library preparation and pooled to equimolar amounts and analysed using PE150 sequence run using an Illumina MiSeq. Sequence analysis was essentially performed using the various packages with the BBMap suite. The generated contig sequence was manually checked using integrative genomics viewer (IGV) software and compared to the sequence of the respective cDNA.

Animal study design

Ten female Dutch domestic goats 2–3 years old were randomly allocated to one of two groups. The Netherlands is free of PPRV and all goats tested negative for PPRV antibodies. For inoculation, the animals were anaesthetized using a mixture of medetomidine and ketamine (intramuscular injection with 2 and 0.5 ml per 100 kg body weight, respectively), after which 5×10^4 $TCID_{50}$ of the virus (rPPRV/Nigeria-EGFP[3] or rPPRV/Tbilisi-EGFP[3]) was inoculated intratracheally (IT) in 5 ml PBS. After inoculation the effect of medetomidine was antagonized by intramuscular injection with atipamezole (0.25 ml per 100 kg body weight). Animals were evaluated daily for clinical signs and rectal temperatures were measured throughout the study [0–20 days post-inoculation (dpi)]. EDTA blood, throat, nose, eye and rectal swabs were taken daily between days 0 and 10, and on days 12, 14, 17 and 20. On days 0, 7, 8, 9, 10, 12, 14, 17 and 20 an additional blood sample for serum was taken. Animals were killed by exsanguination under medetomidine/ketamine anaesthesia. Macroscopic fluorescence was visualized using a custom-made lamp of six 5 V LEDs (Luxeon Lumileds, Lambertian, cyan, peak emission 490–495 nm) mounted with D480/40 bandpass filters (Chroma) [42]. Photographs were taken using an SLR camera with a Dark Reader camera filter (Clare Chemical Research).

Clinical evaluation

We used the clinical score list of Pope *et al.* [19] to monitor PPR-specific clinical signs. These authors developed a clinical score sheet suitable for grading from mild to severe PPRV infections during pathogenesis studies. In brief, on a daily basis, scores of 0–4 were given for the categories general signs, pyrexic response, ocular/nasal discharge, facial mucosal lesions, faeces and respiratory symptoms. The sum of the scores for the different categories was the total clinical score. Note that the sum clinical score as shown in Fig. 2(d) also includes the body temerature data shown in Fig. 2(b). In our study none of the

animals reached the humane endpoints (HEPs). Note that we killed the animals with the most severe clinical signs at 7 and 10 dpi, and it is impossible to predict if these animals would have reached their HEPs if they had been alive for a longer period.

Tissue sampling

Tissue samples for histopathology and immunohistochemistry were collected in 10% neutral buffered formalin and routinely processed into paraffin blocks. Tissue samples for immunofluoresence on cryostat sections were embedded in cryomoulds using OCT compound (TissueTek, Sakura Finetek), snap frozen in liquid nitrogen and stored at −80 °C. For flow cytometric evaluation, lymphoid tissues were collected in PBS and processed into single cell suspensions. A bronchioalveolar lavage (BAL) with PBS was obtained from all animals postmortem and further processed for flow cytometric evaluation. Tissues for PCR and virus isolation were collected and stored directly at −80°C.

Flow cytometry

PBMCs were isolated by gradient separation using lymphoprep (Stemcell). Briefly, 6 ml of whole blood was overlaid on 5 ml of lymphoprep and centrifuged for 30 min at 2000 r.p.m. The lymphocyte layer was isolated and washed three times with PBS. Upon necropsy single cell suspensions from lymphoid tissues were generated by cutting tissues into small pieces and processing it through a 100 µm cell strainer (Corning). Cells were washed once in RPMI medium containing 5% FBS and then resuspended in PBS. Frequencies of infected cells in isolated PBMCs and lymphoid tissues were detected as EGFP-expressing cells by flow cytometry using a Millipore Guava easyCyte flow cytometer. Data were analysed using Millipore Guava soft or FlowJo V7 software.

Processing of EDTA blood samples and swabs for RT-PCR

Samples of EDTA blood and swabs were examined for PPRV RNA by a real time RT-PCR test as described previously [43]. Ct values were calculated; samples without a Ct value showing an increase in the $OD_{640/530}$ were interpreted as Ct40 and negative samples were set at Ct45.

Serology

Sera were examined for PPRV antibodies against the N-protein with the commercial PPR competitive ELISA (ID Screen PPR Competition; ID Vet). OD values were converted to percentage inhibition (PI) using the following formula: PI=100×(OD sample/ OD negative control). The percentage of blocking was displayed as 100 minus this value. The threshold for seropositivity was >50% as recommended by the manufacturer. Sera were also examined for neutralizing antibodies (nAbs) by a virus neutralization (VN) test [44]. Briefly, sera were heat-inactivated (30 min, 56 °C), and twofold serial dilutions of 50 µl from 2 to 2048 were made in minimal essential medium (MEM; Sigma) with antibiotics and FBS. Diluted sera were incubated with an equal volume of 100–300 $TCID_{50}$ of rPPRV/Tbilisi-EGFP[3]. After 1 h at 37 °C, 10^4 VDS cells in 50 µl MEM were added per well and incubation was continued. Wells were scored for fluorescence and CPE. The nAb titre was expressed as the highest dilution showing more than 50% fluorescence neutralization.

Virus isolation

Due to availability and >90% sequence identity between dog and goat nectin-4, virus isolation on swabs was performed on VN4 cells. All nasal swabs were titrated, while for anal, throat and eye swabs only samples with Ct values of <25 by PCR testing were titrated.

Histopathology

Paraffin blocks were cut at 4 µm thickness and sections were collected on coated glass slides (Superfrost Plus; Thermo Fischer). Sections were stained routinely with haematoxylin-eosin stain (HE) or immunostained for GFP or PPRV nucleoprotein (NP). For GFP immunostaining, heat-induced epitope retrieval was applied by heating sections for 5 min at 121 °C in citrate buffer pH 6.0 (Vector laboratories). Rabbit anti-GFP (Invitrogen, dilution 1:200) was used as primary antibody followed by incubation with horse anti-rabbit poly AP (ImmPRESS; Vector Laboratories). A red colour was developed with ImmPACT Vector Red (Vector Laboratories). For the immunostaining of PPRV NP, sections were enzymatically pretreated with 0.1% Proteinase K in TBS for 30 min at 37 °C. The primary antibody was an in-house produced mouse monoclonal antibody (mAb 909-29 dilution 1:100) directed to the NP of CDV, which was shown to cross-react with the NP of PPRV. Goat anti-mouse poly HRP (Superboost; Invitrogen) was used as a secondary antibody and a brown colour was developed with diaminobenzidine (Dako DAB+; Agilent).

For double immunostaining, cryostat sections were cut at 6 µm thickness, collected on coated glass slides (Superfrost Plus; Thermo Fischer) and allowed to dry for 30 min. Sections were then fixed for 10 min in methanol, rinsed in TBS and incubated with one of the following monoclonal antibodies: anti-CD2, anti-CD8 or anti-MHC II (Novus Biologicals, dilution 1:100). Goat anti-mouse IgG Alexa Fluor 545 Tyramide Superboost (Invitrogen) was used for visualization of the cell markers. Sections were then heated in citrate buffer pH 6.0 for 10 min to abolish the tyramide and peroxidase used in the first step. Subsequently, sections
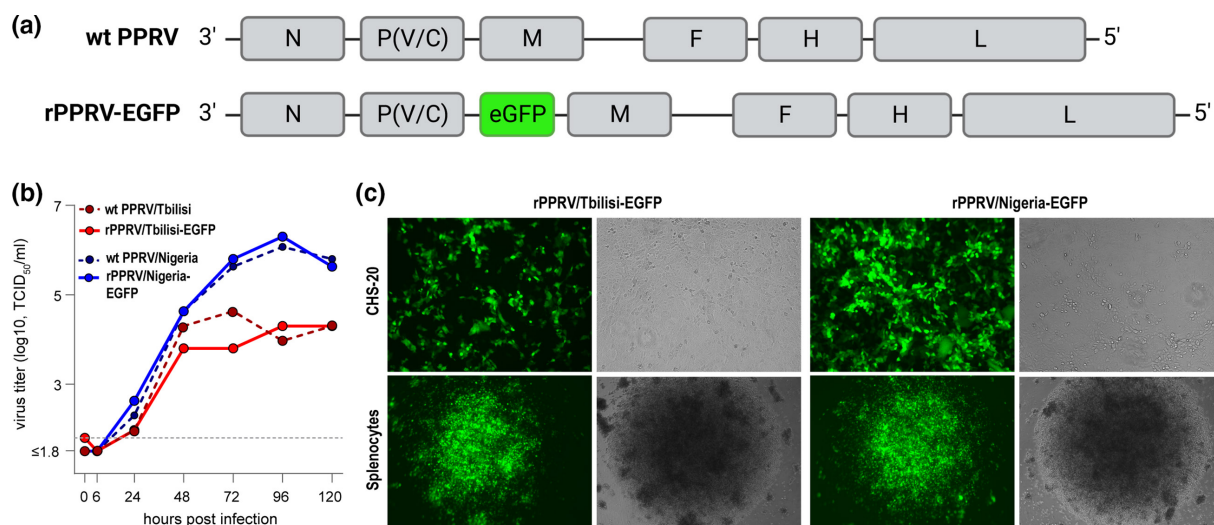
Fig. 1. Design of rPPRV-EGFP and *in vitro* characterization. (a) Schematic overview of wild-type (wt) and recombinant PPRV genome expressing EGFP as an additional transcription unit on position 3 of the genome (rPPRV-EGFP). (b) Comparative growth curves of rPPRV-EGFP and their parental non-recombinant strains in CHS-20 cells. (c) Phenotypic evaluation of rPPRV-EGFP strains in CHS-20 cells (top) and primary goat splenocytes (bottom) at 48 hpi for rPPRV/Tbilisi-EGFP (two left) and rPPRV/Nigeria-EGFP (two right). Each image is displayed in the GFP (left) and brightfield (right) channel. CHS-20: 10x objective; splenocytes: 4x objective.

were incubated with rabbit anti-GFP (Invitrogen, dilution 1:200) followed by goat anti-mouse IgG Alexa Fluor 488 Tyramide Superboost (Invitrogen) and finally mounted in ProLong anti-fading mountant (Vector Laboratories).

RESULTS

Design of rPPRV–EGFP viruses and *in vitro* characterization

We designed, cloned, rescued and sequenced recombinant PPRVs expressing EGFP from an additional transcription unit inserted at position 3 of the genome (Fig. 1a). Reverse genetics for PPRV has been previously described for PPRV vaccine strain Nig75/1 (accession number X74443.2) [44]. Full-length cDNA of the virulent PPRV strain Georgia/Tbilisi/2016 (accession number MF737202) with or without the EGFP cassette and flanked ribozyme sequences under control of both P_{HCMV} and P_{T7} promoters were constructed. Virus rescue was successful at first attempt in VDS cell monolayers using N, P and L expression plasmids derived from PPRV/Nig75/1 and irrespective of prior fowlpox virus (FPV)-T7 infection. However, preliminary results suggested that PPRV rescue was more efficient in the presence of FPV-T7. Rescued viruses were named rPRRV/Nigeria-EGFP, rPPRV/Tbilisi and rPPRV/Tbilisi-EGFP. Sequences of rescued viruses were confirmed by full genome sequencing.

Growth curves performed in CHS-20 cells showed comparable kinetics for each PPRV strain with or without EGFP insertion, suggesting no influence of the additional EGFP cassette (Fig. 1b). Both EGFP-expressing PPRV strains induced morbillivirus-typical syncytia in CHS-20 cells and disseminated well through activated splenocyte cultures (Fig. 1c). This was slightly less apparent for the virulent strain after infection of lymph node cells isolated from the intestine of a healthy goat. We concluded that both recombinant EGFP-expressing viruses have a typical morbillivirus phenotype and are comparable to the viruses not harbouring an additional transcription unit, making them suitable candidates for *in vivo* experiments.

Clinical manifestations of PPR

Two groups of five goats were IT inoculated with the virulent virus rPPRV/Tbilisi-EGFP or vaccine-based virus rPPRV/Nigeria-EGFP, respectively (Fig. 2a). We assessed the general health status, body temperature, systemic infection and haematological changes, as well as virus secretion over a time course of 20 days. Goats were killed at indicated time points chosen as representative time points for the expected peak of infection (day 7/8), declining viraemia (day 10), depletion of immunological structures (day 14) and re-population of immunological structures (day 20/21).

All animals inoculated with the virulent strain had elevated body temperatures starting 4 dpi, while animals inoculated with the vaccine strain retained their pre-inoculation body temperature (Fig. 2b). Specifically, one goat reached a body temperature of 41.5 °C on day 10. This animal was less active and presented with nasal discharge and watery diarrhoea. To minimize animal discomfort, this goat was chosen to be killed at day 10. Moreover, all goats inoculated with the virulent strain showed leukodepletion starting from day 4, as indicated by the decreasing relative white blood cell (WBC) count (Fig. 2c). The WBC count of most
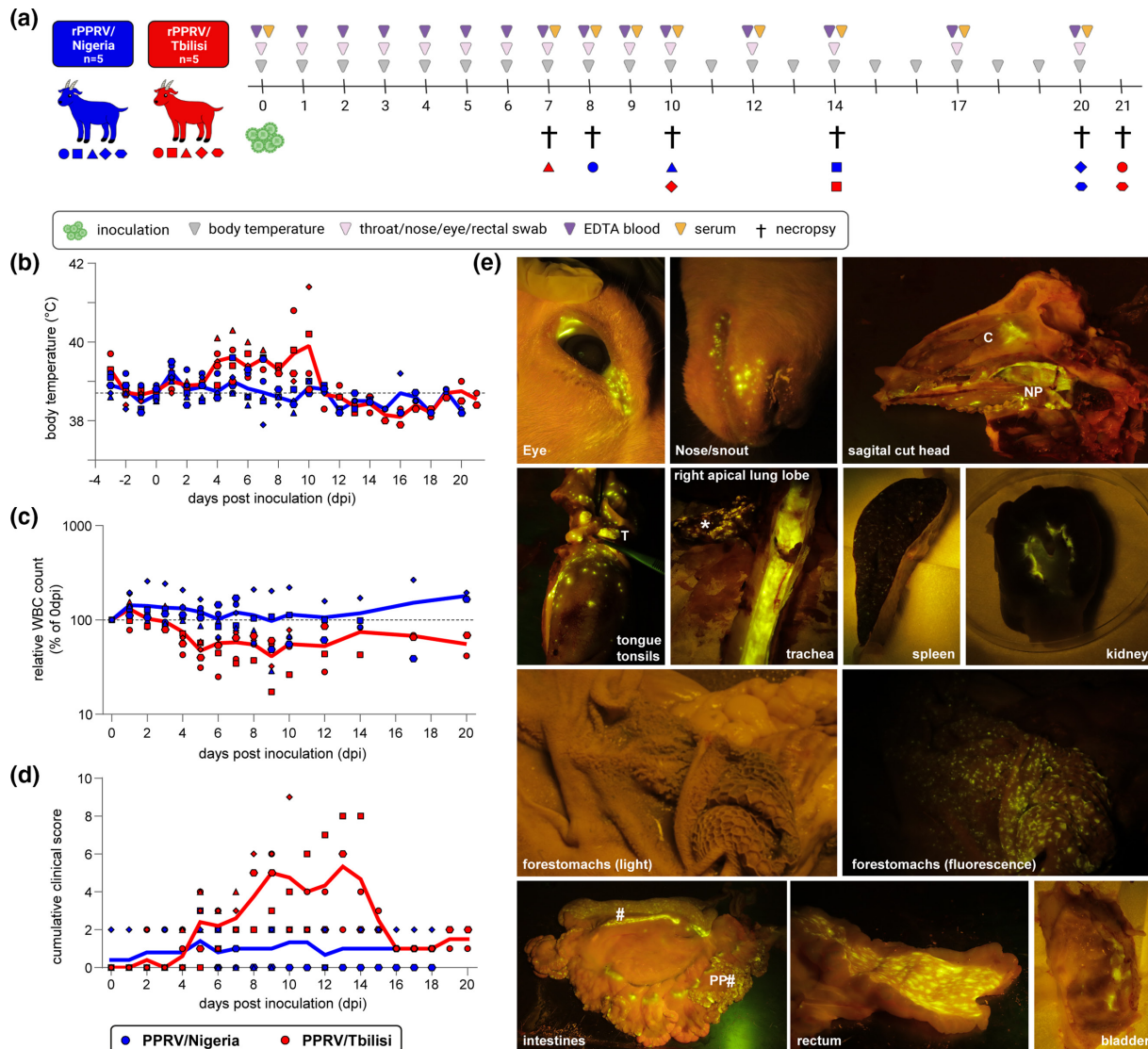
Fig. 2. Study design, clinical data and macroscopic evaluation. (a) Schematic overview of the study design. (b–d) Longitudinal measurement of body temperature (b), white blood cell (WBC) count (c) and cumulative clinical score (d) in goats inoculated with rPPRV/Nigeria-EGFP (blue) or rPPRV/Tbilisi-EGFP (red). Symbols represent individual goats and are consistent throughout the paper. (e) Macroscopic evaluation of a goat inoculated with rPPRV/Tbilisi-EGFP 7 days post-inoculation (dpi). Images show green fluorescent virus-infected cells in the conjunctiva, third eyelid and canthus of the eye, the skin of the nose and lips, as well as the conchae (C) and nasopharynx (NP) (top). Fluorescent virus-infected cells were also detected in the tongue, associated tonsils (T), trachea, diffusely in the right apical lung lobe (*), and in spleen and renal pelvis (medium top). The forestomachs except for the abomasum showed fluorescence (medium bottom), and Peyer's patches (PP), gut-associated lymphatic tissues (GALT, #) of the small and large intestine as well as the rectum and bladder were EGFP-positive (bottom).

animals recovered slowly towards day 14 but did not reach pre-inoculation levels until the end of the study. Animals inoculated with the vaccine strain did not have overall decreased WBC counts. One animal presented with a transient decrease between 8 and 12 dpi, while another animal of the same group had higher WBC counts throughout the study than recorded on day 0, but no general trend of leucopaenia was observed.

Overall animal welfare was monitored daily, and a cumulative clinical score was recorded based on general signs/activity, fever, ocular and nasal discharge, facial mucosal lesions, faeces and respiratory symptoms (Fig. 2d). Some animals presented with nasal and/or ocular discharge from the beginning of the study, leading to a baseline cumulative clinical score of 2 for those. While there was no change of clinical signs in the vaccine virus-inoculated group, animals inoculated with rPPRV/Tbilisi-EGFP rapidly increased in clinical score from 5 dpi onwards. Two animals reached an overall clinical score ≥8, characterized by general

inactivity, fever, watery ocular discharge and mild conjunctivitis as well as diarrhoea. In combination with the decreased WBC, rPPRV/Tbilisi-EGFP inoculated animals presented with typical PPR clinical signs.

Macroscopic evaluation of rPPRV-inoculated goats

Green fluorescence, indicative of PPRV infection, was first detected macroscopically at the eye, tongue and snout 5 dpi with rPPRV/Tbilisi-EGFP. Upon euthanasia of a goat on day 7, we macroscopically assessed lesions and virus-infected cells. Despite abundant presence of EGFP-expressing virus-infected cells in almost all organs, no macroscopic lesions were observed (Fig. 2e). Fluorescence was seen in the conjunctiva, third eyelid and canthus of the eye, the skin of the nose and lips, mucosa of the mouth, tongue and orophaynx as well as the mucosa of the respiratory tract including conchae, nasopharynx, trachea and bronchi. The right apical lobe of the lung showed a chronic pneumonia (as is commonly seen in sheep and goats) and strong diffuse fluorescence. In addition, the mucosa of the renal pelvis, bladder and the gastro-intestinal tract (except for the abomasum) showed fluorescence. The small and large intestine had a distinct fluorescence pattern, potentially indicating the infection of Peyer's patches and gut-associated lymphatic tissues (GALT). Other lymphoid structures such as tonsils, thymus, spleen, tracheo-bronchial, mesenteric and various peripheral lymph nodes were also positive for EGFP. In contrast, the animal inoculated with the vaccine strain and killed 8 dpi had almost no macroscopically visible fluorescence. Only a single EGFP-positive spot of approx. 1 mm was seen on the tongue, gingiva and rumen (data not shown). Macroscopic fluorescence declined with time after inoculation. While there was no macroscopic fluorescence detectable for goats inoculated with rPPRV/Nigeria-EGFP at any additional time point, we still saw fluorescence signal on the eye, nose and snout, tongue, trachea, lung as well as intestine on day 10 and some individual spots on day 14 in goats inoculated with the virulent strain (data not shown).

PPRV excretion and serology

As expected from the macroscopic evaluation, all rPPRV/Tbilisi-EGFP-inoculated goats shed PPRV from their throat, nose, eye and rectum. PPRV genomes were detectable by RT-PCR from 4 dpi onwards in all swab types and animals (Fig. 3a–d). Genome loads peaked on day 8 for nose and eye swabs, day 9 for throat swabs and day 10 for rectal swabs. Genome loads stayed high in rectal swabs, but also did not decrease completely in all other swab types until the end of the study. For four out of 5 animals inoculated with PPRV/Nigeria-EGFP, PPRV genomes could be detected by RT-PCR in at least one swab type at one time point, albeit at low levels. However, PPRV could not be isolated from any of those swabs. In contrast, PPRV/Tbilisi-EGFP was isolated from all swab types for multiple goats and at multiple time points. Viral loads were lowest and detectable for shorter time periods in nose and rectal swabs and no virus could be isolated after 12 dpi (red dotted lines in Fig. 3a–d). Independent of the virus strain used for inoculation, all animals seroconverted (Fig. 3e, f). In a commercial blocking ELISA, almost all animals had detectable antibodies by day 7 (Fig. 3e). Virus-neutralizing antibodies against rPPRV/Tbilisi-EGFP were detectable earlier for rPPRV/Tbilisi-EGFP-inoculated animals than for rPPRV/Nigeria-EGFP-inoculated animals (4/5 vs. 1/5 on day 7) (Fig. 3f). Eventually, all animals from both groups had high virus-neutralizing titres, indicating no qualitative difference in the induction of antibodies.

Infection of lymphoid tissues

Next to PPRV excretion, we evaluated the systemic spread and the involvement of lymphoid tissues in PPRV infection (Fig. 4). PPRV-genomes were detected in EDTA blood of rPPRV/Tbilisi-EGFP-inoculated goats from 4 dpi onwards and genome loads peaked at 7 dpi (Fig. 4a). PPRV genomes could only be detected in EDTA blood of one vaccine strain-inoculated goat on days 8 and 9. PPRV infection in PBMCs analysed by flow cytometry showed a similar trend. rPPRV/Tbilisi-EGFP-inoculated goats became viraemic between days 3 and 5 and infection of PBMCs increased until day 7 or 8, indicated by the percentage of EGFP-positive cells. Peak infections differed between 2.3 and 8.5% and then declined to 0.13% towards the end of the study (20 dpi). Four of five rPPRV/Nigeria-EGFP-inoculated goats had detectable levels of infection in PBMCs between days 6 and 8, albeit to a much lower extent. Maximum infection reached 0.03% of total isolated PBMCs in one animal.

Upon necropsy, we assessed the infection levels in single cell suspensions of multiple lymphoid organs and the lungs by performing post-mortem BAL of the right apical lobe (Fig. 4b). Generally, infection levels were higher than in PBMCs but declined over time. At the peak of infection, 79 and 4.7% of BAL cells were positive for rPPRV/Tbilisi-EGFP and rPPRV/Nigeria-EGFP, respectively. While most peripheral lymph nodes, tonsils and Peyer's patches showed between 0.1 and 0.5% rPPRV/Nigeria-EGFP infection, this was 10 times lower in the thymus and the prefemoral LN. All animals inoculated with the virulent PPRV strain experienced extensive infection of their lymphoid organs. At the peak of infection, infection percentages of most peripheral lymph nodes exceeded 30% and only declined slowly over time. Importantly, the two animals killed on day 20 had not yet cleared their infection.

We performed histopathological analysis of multiple lymphoid tissues to further elucidate rPPRV/Tbilisi-EGFP spread and associated lesions at multiple time points (Fig. 4c). At 7 dpi numerous lymphocytes in the T-cell areas and within the lymphoid follicles were positively stained for GFP. We noted depletion of lymphoid follicles. Importantly, during peak infection (7 dpi) the follicle structure was intact but became depleted at later time points when some follicles contained only a few lymphocytes in the germinal centres. The start of lymphoid depletion was detected 10 dpi, where we still observed PPRV infection of lymphocytes. Infected cells were absent 14 dpi, coinciding with high aAbs in all animals and deteriorated follicles. By 20 dpi the normal follicular
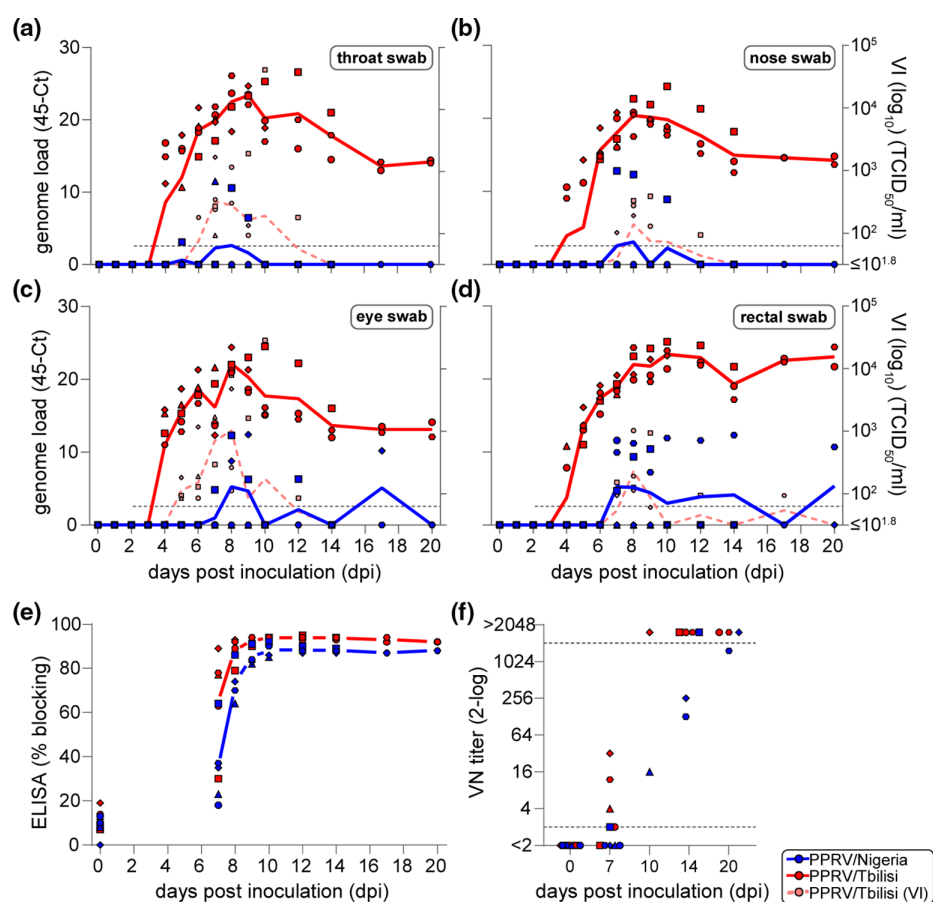
Fig. 3. Viral excretion and serology. (a–d) Longitudinal measurement of PPRV genome or infectious virus in throat (a), nose (b), eye (c) and rectal (d) swabs in goats inoculated with rPPRV/Nigeria-EGFP (blue) or rPPRV/Tbilisi-EGFP (red). Genome loads are plotted on the left *y*-axis, and infectious virus (virus isolation, VI) on the right *y*-axis. The grey dotted line indicates the lower limit of detection for virus isolation. (e–f) PPRV-specific blocking antibodies (e) and rPPRV/Tbilisi-EGFP-neutralizing antibodies (f) over time measured in goats inoculated with rPPRV/Nigeria-EGFP (blue) or rPPRV/Tbilisi-EGFP (red). Symbols represent individual goats and are consistent throughout the paper.

structure was restored, which matched the partial restoration of total WBC counts (Fig. 2c). In contrast, no histological alterations were seen at any stage in the lymphoid tissues of the rPPRV/Nigeria-EGFP-inoculated goat while only a few lymphocytes in tonsils and lymph nodes stained positively for GFP at 8 dpi but no later stages (Fig. S2A, B).

Lastly, we further phenotyped the infected lymphocytes in rPPRV/Tbilisi-EGFP-inoculated goats in various lymphoid tissues including the pharyngeal tonsil, thymus and Peyer's patches (Fig. 4d). Infected cells observed in the T-cell zones of lymph nodes and the thymus co-expressed CD2, a cell adhesion molecule found on T cells and NK cells. Moreover, some infected cells also co-expressed CD8, a marker for cytotoxic T cells. Lymphocytes in primary and secondary lymphoid follicles in the tonsils and lymph nodes were also infected, and EGFP immunoreactivity was co-expressed with MHC class II reactivity, indicative of B lymphocytes. We detected multinucleated giant cells in those lymphoid tissues which were found to be both of T- and B-cell origin. Interestingly, in the chronically inflamed right apical lung lobe, MHC class II staining as a marker for alveolar macrophages/ dendritic cells also showed co-localization with EGFP staining. However, the staining pattern of EGFP in these macrophages did not include the entire cytoplasm but consisted of small spots in the cytoplasm, indicative of phagocytized cellular debris of infected cells rather than direct infection of macrophages.

Overall, we show that the virulent and the vaccine strain spread systemically in goats, albeit at different levels. rPPRV/Tbilisi-EGFP infection of lymphoid tissues caused transient lymphodepletion, which was largely restored at day 20. Infected cell types included T and B cells, and may have included MHC class II-expressing antigen-presenting cells.

Infection of epithelia

We further investigated the infection of epithelia in rPPRV/Tbilisi-EGFP-inoculated goats. No gross pathological lesions were seen during the peak of infection, despite immense infection demonstrated by the macroscopic fluorescence (Fig. 2e). Upon
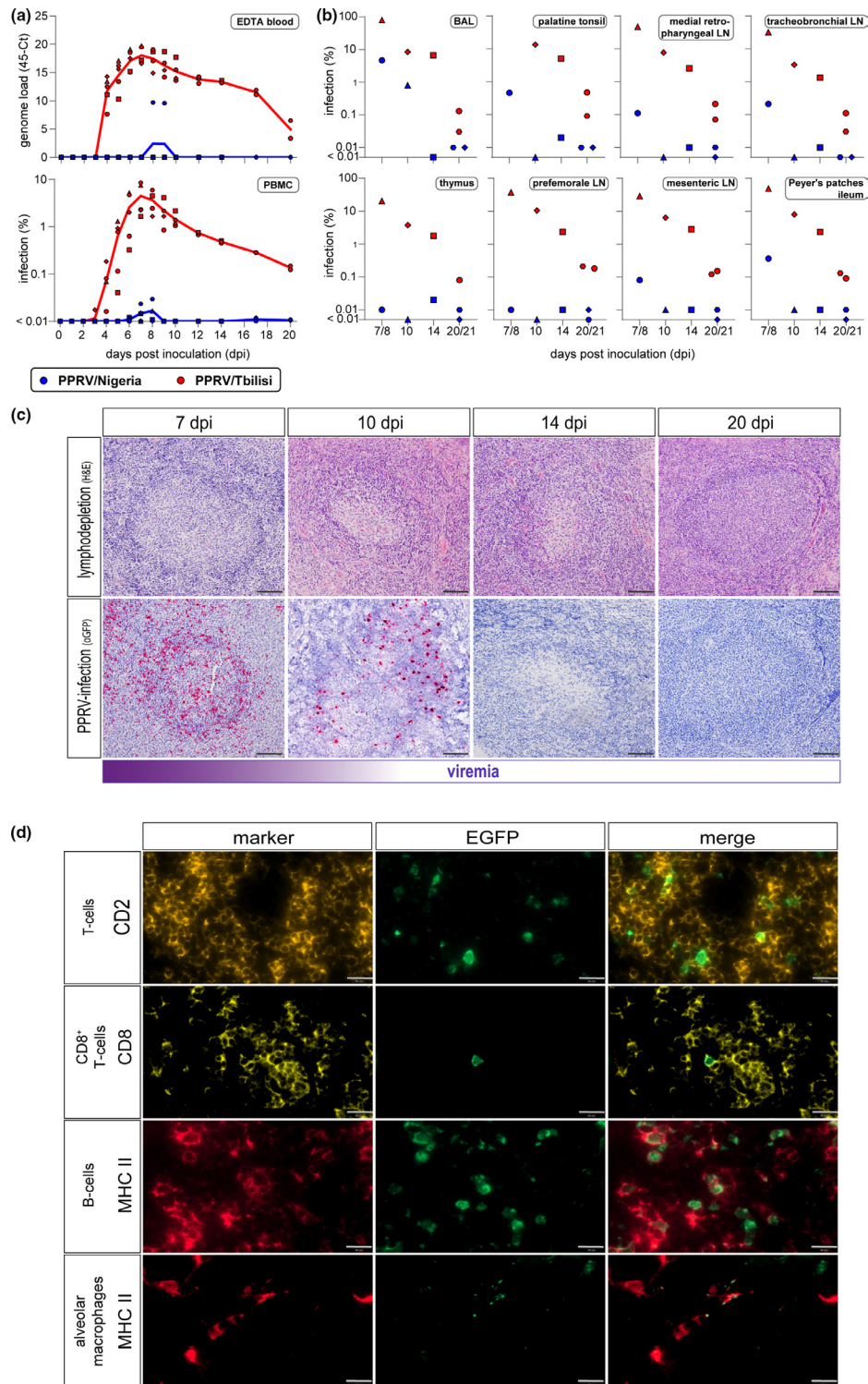
Fig. 4. Systemic spread of rPPRV-EGFP and characterization of infected lymphocytes. (a) Viraemia measured as genome loads in EDTA blood by RT-PCR (top) and percentage EGFP-expressing lymphocytes by flow cytometry (bottom). Lines represent the mean and geometric mean, respectively. (b) Flow cytometric evaluation of rPPRV-EGFP infection of bronchioalveolar lavage (BAL) and single cell suspensions of various lymphoid tissues. Symbols and colours represent individual goats and are consistent throughout the paper. (c) Representative images of longitudinal evaluation of lymphoid follicles in the palatine tonsil using H&E (top) and immunohistochemistry (anti-GFP; bottom) to evaluate lymphodepletion and rPPRV/Tbilisi-EGFP infection. Bar, 100 µm. (d) Phenotyping of rPPRV-EGFP-infected cells (green) using the T-cell marker CD2 in the pharyngeal tonsil (top), CD8 in the thymus (second), and B-cell and alveolar macrophage marker MHC class II in the Peyer's patches of the caecum and lung, respectively (bottom two). Phenotypic characterization was based on the expressed marker and location in tissue. Bar; 20 µm.
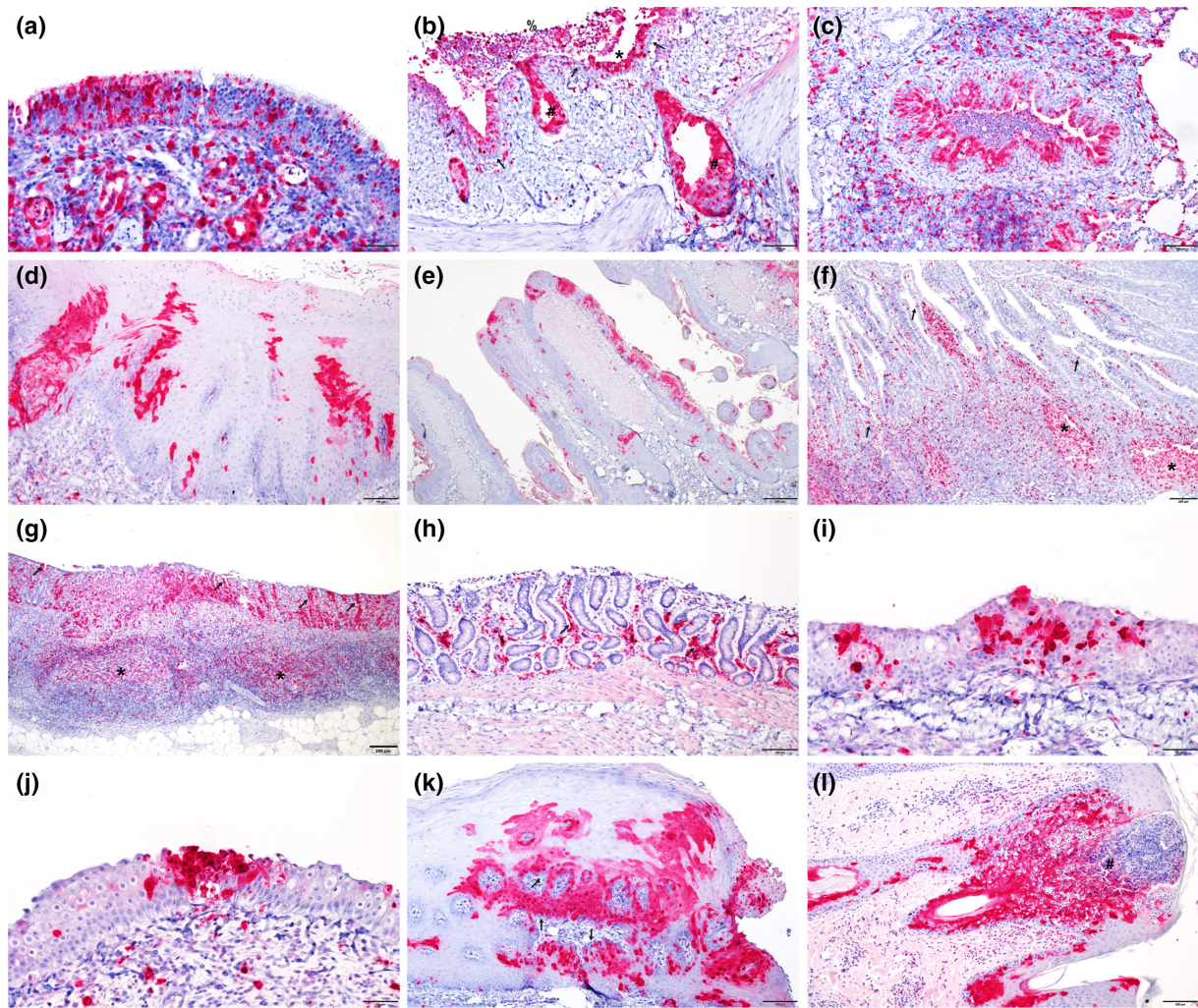
Fig. 5. Histopathology of the various epithelia in an rPPRV/Tbilisi-EGFP-inoculated goat at 7 dpi. Immunohistochemical staining for GFP. (a–c) Respiratory tract. (a) Positive staining of the pseudostratified columnar ciliated epithelium of the conchae. The epithelial layer of the nasal glands and scattered lymphoid cells in the submucosa are also positively stained. (b) Bronchus with staining of the luminal epithelial layer (*) and glandular epithelium (#) of the mucous glands in the submucosa. This panel shows sloughing and debris of epithelial cells in the lumen (%) but an intact stratum basale (arrows). (c) Chronic bronchopneumonia of the right apical lobe. Staining of the bronchiolar epithelium as well as the type 2 cuboidal epithelium of the alveoli. The bronchus-associated lymphoid tissue (BALT) is hyperplastic with scattered GFP-positive lymphocytes in the follicles. (d–h) Gastro-intestinal tract. Squamous epithelium of the mouth (d) and reticulum (e) and the columnar epithelium of the ileum (f), caecum (g) and rectum (h) are positively stained (arrows). The caecal epithelium shows a much heavier staining compared to the ileal and rectal epithelium. Panels also show heavy infection of MALT (*) in the ileum and caecum and scattered infected lymphocytes in the lamina propria. (i–j) Urinary tract. Staining of the transitional epithelium of the renal pelvis (i) and the bladder (j). (k–l) Integumentary system. Skin with extensive infection of the squamous epithelium and relative sparing of the stratum basale (arrows) (k). Infiltration of the dermis and epidermis by PMNs leading to a micro-abscess (#) in the epithelium (l). Bar, 50 µm (a, i, j), 100 µm (b, c, d, h, k, l), 200 µm (f, g) or 500 µm (e).

histopathological evaluation using haematoxylin and eosin (H&E), together with anti-EGFP and anti-NP staining, we confirmed infection of epithelia and associated glands at 7 dpi in various tissues in the respiratory tract [nose, conchae (Fig. 5a), nasopharynx, trachea, bronchi (Fig. 5b) and lung (Fig. 5c)], in the gastro-intestinal tract [mouth (Fig. 5d), oropharynx, forestomaches (Fig. 5e), but not the abomasum, small intestine (Fig. 5f), large intestine (Fig. 5g) or rectum (Fig. 5h)], in the urinary tract [renal pyelum (Fig. 5i) and bladder (Fig. 5j)] and in the conjunctiva and skin (Fig. 5k). Occasionally, an influx of polymorphonuclear leukocytes (PMNs) could be detected at sites with degeneration/necrosis of epithelial cells sometimes leading to micro-abscesses in the epithelium (Fig. 5l). Morbillivirus-specific multinucleated giant cells were abundantly present in lymphoid (Fig. 6a, d) as well as epithelial structures (Fig. 6b, e). In addition, eosinophilic intracytoplasmic inclusion bodies could be seen within epithelial cells especially in the forestomach (Fig. 6c, f). The epithelium of the caecum was highly infected (Fig. 7a, d) and multiple histo-pathological changes could be observed. These included acute typhlitis with necrosis of the crypt epithelium, influx of PMNs
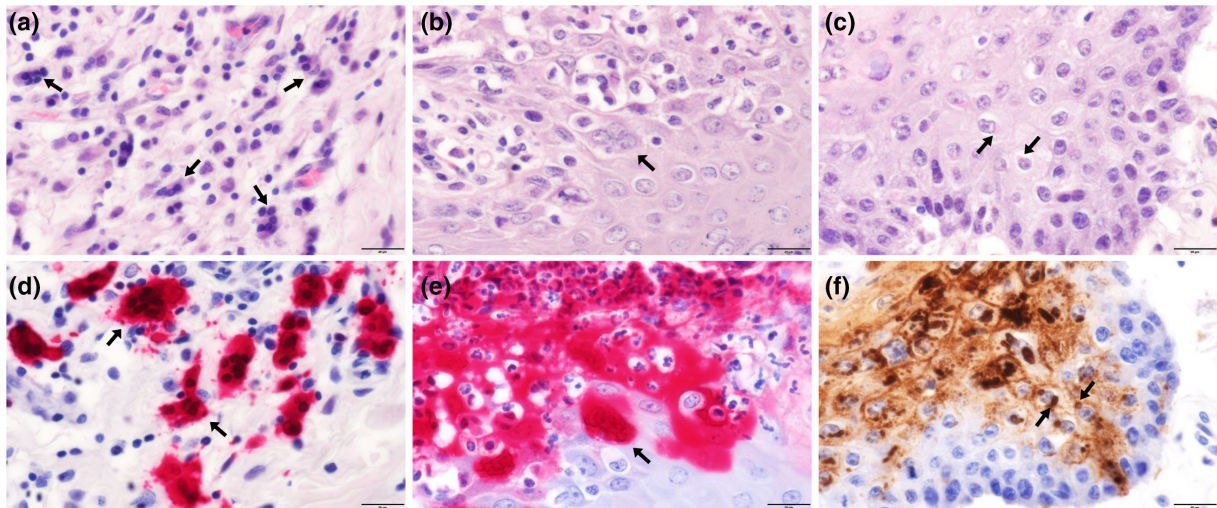
Fig. 6. Syncytia and inclusion bodies in an rPPRV/Tbilisi-EGFP-inoculated goat at 7 dpi. (a–c) Haematoxylin and eosin staining. (d–f) Serial sections of (a)–(c) immunostained for EGFP (d, e) or PPRV NP (f).(a, d) Numerous lymphoid-derived syncytia (arrows) in the submucosa of the conjunctiva of the third eyelid. (b, e) Epithelial-derived syncytia (arrow) in the squamous epithelium of the skin. (c, f) Eosinophilic intracytoplasmic inclusion bodies (arrows) in the epithelium of the omasum. The inclusion bodies stain strongly for the NP. Note also the strong immunolabelling of the cell membranes of the keratinocytes. Bar, 20 µm.

sometimes leading to crypt abscesses and loss of the surface epithelium. Interestingly, other parts of the intestines such as the small intestine and rectum mainly showed infection of lymphoid cells in the lamina propria, but only rarely in epithelial cells. In rPPRV/Nigeria-EGFP-inoculated goats, a few epithelial cells in the oral mucosa were positively stained for GFP at 8 dpi but no infection of other epithelia was seen at 8 dpi or any later stage (Fig. S2C–I).

Pathological changes in large intestine of rPPRV/Tbilisi-EGFP-inoculated goats at day 14: Zebra stripes

While macroscopic lesions at the peak of infection were absent, a goat inoculated with the virulent PPRV strain and necropsied at 14 dpi presented with pathognomonic 'zebra stripes', macroscopic mucosal alterations located at the transition from caecum
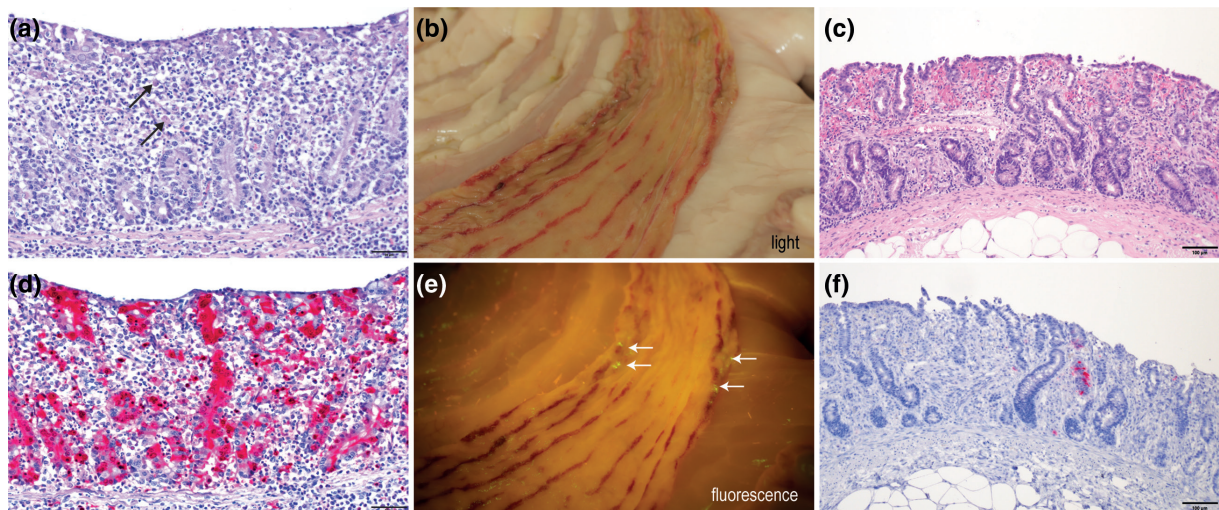

Fig. 7. Pathology of the caecum in rPPRV/Tbilisi-EGFP-inoculated goats. (a, d) Acute typhlitis with degeneration/necrosis of epithelial cells (arrows), influx of PMNs in the lamina propria and loss of the surface epithelium at 7 dpi (a). Epithelial cells stain heavily for EGFP as do scattered lymphocytes in the lamina propria (d). (b, e) Macroscopic evaluation of PPRV-typical zebra stripes displayed as photos using regular light (b) or handlamp for illuminating EGFP fluorescence (e) at 14 dpi. Arrows indicate green fluorescent spots. (c) Microscopic examination shows haemorrhages in the upper lamina propria and loss of crypts. (f) Only a few epithelial cells show positive staining for GFP at this stage. Bar, 50 µm (a,d) or 100 µm (c,f).

to colon ascendens (Fig. 7b), an area which was strongly infected and showed microscopic signs of acute typhlitis during the peak of infection in a different goat (Fig. 7a, d). Interestingly, zebra stripes did not directly overlap with macroscopically visible fluorescent areas of infection, which were scarce at this point in time (Fig. 7e). Microscopically, mucosal alterations at 14 dpi consisted of loss of crypts, haemorrhages in the upper lamina propria, and oedema (Fig. 7c). Simultaneously, we found evidence of crypt regeneration (characterized by an increased mitosis index in epithelial cells of the crypts) and increased angiogenesis in the lamina propria. At this stage the luminal epithelium was restored and only a few epithelial cells in the crypts stained positive for EGFP (Fig. 7f).

Overall, we observed few macroscopic pathological lesions during the peak of infection, despite abundant infection of lymphoid and epithelial tissues at that time. This was followed by systemic and local lymphodepletion, coinciding with decreasing infection percentages of lymphocytes measured in peripheral blood and lymphoid organs. At 14 dpi, we also observed pathognomonic zebra stripes in the large intestine of a goat that experienced diarrhoea and elevated temperature between 5 and 10 dpi and which was subject to the most severe leukodepletion, long viraemia and late induction of virus-neutralizing antibodies (Figs 2 and 3, red square).

DISCUSSION

Virulent PPR viruses circulate in a large part of the world and cause severe (socio-)economic damage. Moreover, multiple PPR viruses have spread rapidly to new areas in the last decade and PPRV/Georgia/Tbilisi/2016 has even been detected at the border of Europe. Therefore, there is a need for a better understanding of the pathogenesis of PPR disease. We performed an in-depth pathology study of recombinant EGFP-expressing viruses based on PPRV/Georgia/Tbilisi/2016 and an EGFP-expressing vaccine virus. All animals inoculated with the virulent strain showed infection of lymphoid tissues, and the respiratory and alimentary tract. We and others showed PPRV infection caused morbillivirus-typical leucopaenia, locally seen in the depletion of lymphoid follicles [4, 23, 24], and also systemically in a decrease of WBC counts [15, 19, 25, 26].

Transient lymphopaenia is induced by infection of immune cells via its receptor CD150 (SLAM). Previously, PPRV-specific RNA has been detected in whole blood, WBC or serum of experimentally inoculated goats that mostly peaked at the end of the first week post-inoculation [17, 18, 20, 21, 25]. In our study, we quantified the percentage of infected lymphocytes based on the expression of EGFP and confirmed peak infection at 7–8 dpi. With 2.3–8.5% of lymphocytes infected, rPPRV/Tbilisi-EGFP shows resemblance to experimental MeV infection of macaques; in experimental CDV infection of ferrets a much higher percentage of lymphocytes is infected [32, 33, 42]. At the peak of infection, macroscopic evaluation showed exceptionally bright fluorescent lymphoid tissues. Flow cytometry-based quantification of infected cells in peripheral lymph nodes indicated that more than one-third of lymphocytes were infected with rPPRV/Tbilisi-EGFP [24]. Infected lymphocytes were possibly of T-cell and B-cell origin, which was previously shown for PPRV and other morbilliviruses [28, 33]. In other studies, macrophages present in lymph nodes or the lung have also been shown to become infected by PPRV [20, 28]. In our study, alveolar macrophages, a predominant target for MeV in humans [45], were positive for EGFP at day 7 post-PPRV-inoculation, but at this point had potentially only phagocytosed infected cells rather than being infected themselves. Because M2c macrophages express high levels of CD150 and partly reside in the lung, they were suspected to be involved in PPRV infection [24]. However, current evidence argues that M2c macrophages do not play a role in uptake or transmission of PPRV [24]. Yet, the working hypothesis for primary targets of PPRV infection includes cells residing in the lamina propria and submucosa of the lungs, possibly being dendritic cells or subtypes of macrophages other than M2c [19, 20, 24].

It is widely accepted that morbilliviruses infect epithelial cells using nectin-4 receptors after local and systemic replication in lymphoid tissues [19, 24, 46]. We detected fluorescence, indicative of PPRV infection, for a longer period in epithelial tissues when compared to lymphoid tissues. Extensive previous pathological studies describe erosion and necrosis in the upper respiratory tract, signs of pneumonia in the lungs, haemorrhage and congestion in the intestines (possibly meaning PPRV-typical zebra stripes), as well as haemorrhages and inflammation in liver and kidney [23, 24]. With the exception of the detected zebra stripes, we did not see any of those macroscopic pathological changes, indicating that the PPRV strain we used might cause milder clinical symptoms. However, despite the few obvious pathological changes at the peak of infection, the abundant presence of fluorescent tissues indicated that rPPRV/Tbilisi-EGFP infection caused a systemic infection with a potential for a severe outcome. Interestingly, although all stomachs except the abomasum were macroscopically and microscopically positive for the presence of PPRV-infected cells in our study, no or little apparent pathological lesions were reported in the forestomachs by others [23, 24]. Gautam *et al.* also did not detect any PPRV antigen in the abomasum and most PPRV antigen positivity was in the caecal epithelial lining on day 5, potentially facilitating the induction of zebra stripes later as observed by us in the caecum and colon ascendens [24]. The histological alterations found in our study were in line with other reports and were dominated by PMN infiltration, multinucleated giant cells, haemorrhages, degeneration, necrosis and inclusion bodies [20, 23, 24].

We and others used body temperature and overall clinical signs as a measure for severity of disease [19, 21, 22, 25, 26]. PPR symptoms can range from mild to severe and a PPR infection is often lethal. Factors influencing severity of disease include

animal species and breed, age of animals and viral strain differences. Our study investigated the pathogenesis of a recent virulent PPRV strain from Georgia, reported to cause a wide range of clinical signs and a high mortality rate [38], in comparably old goats (2–3 years of age), in which PPRV is suspected to cause milder disease than in young animals. As we killed the goats experiencing most symptoms first to avoid further suffering, we pre-empted humane endpoint criteria. However, it also cannot be excluded that our recombinant viruses were less virulent than the clinical isolates. To our knowledge, no recombinant PPRV harbouring an additional transcription unit (ATU) has been used in pathogenesis studies. Although it is known that adding an ATU (especially before the nucleoprotein, position 1) may alter the morbillivirus-typical transcriptional gradient and therefore potentially attenuate the recombinant virus [32], an *in vivo* study in cattle using recombinant RPV expressing EGFP on position 3 of the genome did not show any differences in pathogenesis compared to the virus without EGFP expression [47]. Moreover, *in vitro* characterization and comparison performed in this study did not hint towards any difference based on the insertion of EGFP in rPPRV/Tbilisi-EGFP, suggesting that the used virus strain and/or age of the animal were responsible for the moderate clinical symptoms observed in our study.

Morbilliviruses are known to induce strong humoral responses after infection or vaccination. However, an early induction of PPRV-specific antibodies at the end of the first week post-infection does not necessarily prevent the animals from dying after a PPRV infection [16]. We measured an early humoral response in both study groups; the response was slightly faster in rPPRV/Tbilisi-EGFP-inoculated animals as compared to vaccine virus-inoculated animals, confirming observations of a faster and stronger immune response in animals that have been inoculated with a more virulent PPRV strain than with a less severe or vaccine strain [16, 25]. In contrast, Rajak *et al.* observed a delayed onset of PPRV-specific and bystander antibodies in goats experiencing severe clinical symptoms, suggesting that the immune system may be impaired during PPRV infection [15].

Independent of the time required to produce antibodies post-inoculation, our data suggest no qualitative difference in virus neutralization between the two groups. Field studies as well as laboratory-controlled experiments moreover confirm protection from clinical disease after infection or challenge with a wild-type virus. These studies evaluated vaccine efficacy in experimental challenge studies and deciphered immunological parameters [26, 30, 31]. In addition, we aimed to understand the tropism of rPPRV/Nigeria-EGFP after IT inoculation. Unlike virulent strains, PPRV vaccine strains are lymphotropic and no longer epitheliotropic *in vivo*, impairing virus transmission [14]. Similarly, live-attenuated measles virus vaccines were identified to predominantly target dendritic cells and macrophages rather than muscle cells when administered intramuscularly [48], and delivery to the respiratory tract resulted in a preferred tropism of myeloid and lymphoid cells and rarely in epithelial cells [49]. In line with this, we noted a short viraemia detected by EGFP expression in no more than 0.03% of PBMCs and were also able to detect rPPRV/Nigeria-EGFP in lymphoid organs at 8 dpi. Importantly, this was not accompanied by clinical signs, altered haematology, or macroscopic or microscopic lesions, making it a valuable and reliable vaccine strain. Others were not able to detect vaccine virus excretion in ocular swabs after vaccination [26], whereas we measured PPRV-genomes in ocular swabs (2/5) and more robustly in rectal swabs (3/5). Importantly, we were not able to isolate rPPRV/Nigeria-EGFP from any swab sample, suggesting that the vaccine virus indeed is not shed to detectable levels.

In conclusion, we have used fluorescence-guided pathology to investigate and compare the tropism and pathogenesis of a virulent PPRV strain from Georgia and PPRV vaccine strain Nigeria/75. The virulent virus caused a self-limiting disease that was more reminiscent of measles in primates than distemper in ferrets, but with a more extensive impact on the digestive tract compared to MeV and CDV. The vaccine virus was shown to cause a systemic infection that did not extensively replicate in lymphoid tissues. The limited reagent availability and biosafety concerns for the environment made the work and characterization of infected cell types more challenging than for other morbilliviruses. Yet, studying PPRV in its natural host is a valuable animal model to further understand morbilliviruses and which will eventually help to recognize, monitor and eradicate PPR disease.

Ethical statement

Animal experiments were conducted in compliance with European regulations on the protection of animals used for scientific purposes (EU directive 2010/63/EU) and Dutch legislation (Experiments on Animals Act, 1977). The procedures were approved by the animal ethics committee of Wageningen Bioveterinary Research (WBVR) and the Dutch Central Authority for Scientific Procedures on Animals (permit number 2019.D-0041.001)

References

1. Baron MD, Parida S, Oura CAL. Peste des petits ruminants: a suitable candidate for eradication? *Vet Rec* 2011;169:16–21.

2. Diallo A, Minet C, Le Goff C, Berhe G, Albina E, *et al.* The threat of peste des petits ruminants: progress in vaccine development for disease control. *Vaccine* 2007;25:5591–5597.

3. Rima B, Balkema-Buschmann A, Dundon WG, Duprex P, Easton A, *et al.* ICTV Virus Taxonomy Profile: Paramyxoviridae. *J Gen Virol* 2019;100:1593–1594.

4. Kumar P, Tripathi BN, Sharma AK, Kumar R, Sreenivasa BP, *et al.* Pathological and immunohistochemical study of experimental peste des petits ruminants virus infection in goats. *J Vet Med B Infect Dis Vet Public Health* 2004;51:153–159.

5. Jones L, Giavedoni L, Saliki JT, Brown C, Mebus C, *et al.* Protection of goats against peste des petits ruminants with a vaccinia virus double recombinant expressing the F and H genes of rinderpest virus. *Vaccine* 1993;11:961–964.

6. Libeau G, Diallo A, Parida S. Evolutionary genetics underlying the spread of peste des petits ruminants virus. *Animal Frontiers* 2014;4:14–20.

7. Bardhan D, Kumar S, Anandsekaran G, Chaudhury JK, Meraj M, *et al.* The economic impact of peste des petits ruminants in India. *Rev Sci Tech* 2017;36:245–263.

8. Jones BA, Rich KM, Mariner JC, Anderson J, Jeggo M, *et al.* The economic impact of eradicating peste des petits ruminants: a benefit-cost analysis. *PLoS One* 2016;11:e0149982.

9. Parida S, Muniraju M, Altan E, Baazizi R, Raj GD, *et al.* Emergence of PPR and its threat to Europe. *Small Rumin Res* 2016;142:16–21.

10. Rajko-Nenow PZ, Cunliffe TG, Flannery JT, Ropiak HM, Avaliani L, *et al.* Complete genome sequence of peste des petits ruminants virus from Georgia, 2016. *Genome Announc* 2017;5:e01091-17.

11. Countries reaffirm political will to globally eradicate Peste des petits ruminants [press release]; 2018 Sep 7. https://www.woah.org/en/countries-reaffirm-political-will-to-globally-eradicate-peste-des-petits-ruminants/

12. OIE. Peste des petits ruminants; 2022. https://www.oie.int/en/disease/peste-des-petits-ruminants/

13. Adu FD, Joannis T, Nwosuh E, Abegunde A. Pathogenicity of attenuated peste des petits ruminants virus in sheep and goats. *Rev Elev Med Vet Pays Trop* 1990;43:23–26.

14. Diallo A, Taylor WP, Lefèvre PC, Provost A. Atténuation d'une souche de virus de la peste des petits ruminants: candidat pour un vaccin homologue vivant. *Rev Elev Med Vet Pays Trop* 1989;42:311–319.

15. Rajak KK, Sreenivasa BP, Hosamani M, Singh RP, Singh SK, *et al.* Experimental studies on immunosuppressive effects of peste des petits ruminants (PPR) virus in goats. *Comp Immunol Microbiol Infect Dis* 2005;28:287–296.

16. Couacy-Hymann E, Bodjo C, Danho T, Libeau G, Diallo A. Evaluation of the virulence of some strains of peste-des-petits-ruminants virus (PPRV) in experimentally infected West African dwarf goats. *Vet J* 2007;173:178–183.

17. El Harrak M, Touil N, Loutfi C, Hammouchi M, Parida S, *et al.* A reliable and reproducible experimental challenge model for peste des petits ruminants virus. *J Clin Microbiol* 2012;50:3738–3740.

18. Hammouchi M, Loutfi C, Sebbar G, Touil N, Chaffai N, *et al.* Experimental infection of alpine goats with a Moroccan strain of peste des petits ruminants virus (PPRV). *Vet Microbiol* 2012;160:240–244.

19. Pope RA, Parida S, Bailey D, Brownlie J, Barrett T, *et al.* Early events following experimental infection with peste-des-petits ruminants virus suggest immune cell targeting. *PLoS One* 2013;8:e55830.

20. Truong T, Boshra H, Embury-Hyatt C, Nfon C, Gerdts V, *et al.* Peste des petits ruminants virus tissue tropism and pathogenesis in sheep and goats following experimental infection. *PLoS One* 2014;9:e87145.

21. Wernike K, Eschbaumer M, Breithaupt A, Maltzan J, Wiesner H, *et al.* Experimental infection of sheep and goats with a recent isolate of peste des petits ruminants virus from Kurdistan. *Vet Microbiol* 2014;172:140–145.

22. Bamouh Z, Fakri F, Jazouli M, Safini N, Omari Tadlaoui K, *et al.* Peste des petits ruminants pathogenesis on experimental infected goats by the Moroccan 2015 isolate. *BMC Vet Res* 2019;15:452.

23. Begum S, Nooruzzaman M, Islam MR, Chowdhury EH. A sequential study on the pathology of peste des petits ruminants and tissue distribution of the virus following experimental infection of Black Bengal Goats. *Front Vet Sci* 2021;8:635671.

24. Gautam S, Joshi C, Sharma AK, Singh KP, Gurav A, *et al.* Virus distribution and early pathogenesis of highly pathogenic peste-des-petits-ruminants virus in experimentally infected goats. *Microb Pathog* 2021;161:105232.

25. Eloiflin R-J, Grau-Roma L, Python S, Mehinagic K, Godel A, *et al.* Comparative pathogenesis of peste des petits ruminants virus strains of difference virulence. *Vet Res* 2022;53:57.

26. Enchery F, Hamers C, Kwiatek O, Gaillardet D, Montange C, *et al.* Development of a PPRV challenge model in goats and its use to assess the efficacy of a PPR vaccine. *Vaccine* 2019;37:1667–1673.

27. Lemon K, de Vries RD, Mesman AW, McQuaid S, van Amerongen G, *et al.* Early target cells of measles virus after aerosol infection of non-human primates. *PLoS Pathog* 2011;7:e1001263.

28. Baron MD, Hodgson S, Moffat K, Qureshi M, Graham SP, *et al.* Depletion of CD8+ T cells from vaccinated goats does not affect protection from challenge with wild-type peste des petits ruminants virus. *Transbound Emerg Dis* 2021;68:3320–3334.

29. Parida SC-H E, Pope RA, Mahapatra M, El Harrak M, Brownlie J, *et al. Pathology of peste des petits ruminants. Peste des Petits Ruminants Virus*. Berlin/Heidelberg, Germany: Springer; 2015, pp. 51–67.

30. Mahapatra M, Selvaraj M, Parida S. Comparison of immunogenicity and protective efficacy of PPR live attenuated vaccines (Nigeria 75/1 and Sungri 96) administered by intranasal and subcutaneous routes. *Vaccines* 2020;8:168.

31. Hodgson S, Moffat K, Hill H, Flannery JT, Graham SP, *et al.* Comparison of the immunogenicities and cross-lineage efficacies of live attenuated peste des petits ruminants virus vaccines PPRV/Nigeria/75/1 and PPRV/Sungri/96. *J Virol* 2018;92:e01471-18.

32. von Messling V, Milosevic D, Cattaneo R. Tropism illuminated: lymphocyte-based pathways blazed by lethal morbillivirus through the host immune system. *Proc Natl Acad Sci* 2004;101:14216–14221.

33. de Swart RL, Ludlow M, de Witte L, Yanagi Y, van Amerongen G, *et al.* Predominant infection of CD150+ lymphocytes and dendritic cells during measles virus infection of macaques. *PLoS Pathog* 2007;3:e178.

34. Nambulli S, Rennick LJ, Acciardo AS, Tilston-Lunel NL, Ho G, *et al.* FeMV is a cathepsin-dependent unique morbillivirus infecting the kidneys of domestic cats. *Proc Natl Acad Sci* 2022;119:e2209405119.

35. Seki F, Ono N, Yamaguchi R, Yanagi Y. Efficient isolation of wild strains of canine distemper virus in Vero cells expressing canine SLAM (CD150) and their adaptability to marmoset B95a cells. *J Virol* 2003;77:9943–9950.

36. Adombi CM, Lelenta M, Lamien CE, Shamaki D, Koffi YM, *et al.* Monkey CV1 cell line expressing the sheep-goat SLAM protein: a highly sensitive cell line for the isolation of peste des petits

ruminants virus from pathological specimens. *J Virol Methods* 2011;173:306–313.

37. Britton P, Green P, Kottier S, Mawditt KL, Penzes Z, *et al*. Expression of bacteriophage T7 RNA polymerase in avian and mammalian cells by a recombinant fowlpox virus. *J Gen Virol* 1996;77:963–967.

38. Rajko-Nenow PZ, Cunliffe TG, Flannery JT, Ropiak HM, Avaliani L, *et al*. Complete genome sequence of peste des petits ruminants virus from Georgia, 2016. *Genome Announc* 2017;5:e01091-17.

39. Kolakofsky D, Pelet T, Garcin D, Hausmann S, Curran J, *et al*. Paramyxovirus RNA synthesis and the requirement for hexamer genome length: the rule of six revisited. *J Virol* 1998;72:891–899.

40. Vieira J, Messing J. New pUC-derived cloning vectors with different selectable markers and DNA replication origins. *Gene* 1991;100:189–194.

41. Wensvoort G, Terpstra C, Bloemraad M. Detection of antibodies against African swine fever virus using infected monolayers and monoclonal antibodies. *Vet Rec* 1988;122:536–539.

42. de Vries RD, McQuaid S, van Amerongen G, Yüksel S, Verburgh RJ, *et al*. Measles immune suppression: lessons from the macaque model. *PLoS Pathog* 2012;8:e1002885.

43. van Rijn PA, Boonstra J, van Gennip HGP. Recombinant Newcastle disease viruses with targets for PCR diagnostics for rinderpest and peste des petits ruminants. *J Virol Methods* 2018;259:50–53.

44. Hu Q, Chen W, Huang K, Baron MD, Bu Z. Rescue of recombinant peste des petits ruminants virus: creation of a GFP-expressing virus and application in rapid virus neutralization test. *Vet Res* 2012;43:48.

45. Allen IV, McQuaid S, Penalva R, Ludlow M, Duprex WP, *et al*. Macrophages and dendritic cells are the predominant cells infected in measles in humans. *mSphere* 2018;3:e00570-17.

46. de Vries RD, Mesman AW, Geijtenbeek TBH, Duprex WP, de Swart RL. The pathogenesis of measles. *Curr Opin Virol* 2012;2:248–255.

47. Banyard AC, Simpson J, Monaghan P, Barrett T. Rinderpest virus expressing enhanced green fluorescent protein as a separate transcription unit retains pathogenicity for cattle. *J Gen Virol* 2010;91:2918–2927.

48. Rennick LJ, de Vries RD, Carsillo TJ, Lemon K, van Amerongen G, *et al*. Live-attenuated measles virus vaccine targets dendritic cells and macrophages in muscle of nonhuman primates. *J Virol* 2015;89:2192–2200.

49. de Swart RL, de Vries RD, Rennick LJ, van Amerongen G, McQuaid S, *et al*. Needle-free delivery of measles virus vaccine to the lower respiratory tract of non-human primates elicits optimal immunity and protection. *NPJ Vaccines* 2017;2:22.